scientific reports

Check for updates

OPEN

Improving preparation and luminescence properties of Eu and dy doped $Sr_2MgSi_2O_7$ phosphors by adding excess silica

Chi Zhang[1]✉, Liuming Wei[2], Qin Liu[5], Ruirui Cui[4], Chaoyong Deng[4]✉ & Jingyu Li[3]✉

Solid state reaction method is most commonly used to synthesize $Sr_2MgSi_2O_7$: Eu^{2+}, Dy^{3+} phosphors. In order to avoid the energy waste caused by high sintering temperature, we systematically studied and optimized the preparation process of $Sr_2MgSi_2O_7$: Eu^{2+}, Dy^{3+} long afterglow phosphors by increasing the Si/Sr ratio in the raw materials. The appropriate addition of silica not only facilitates the preparation of single phase $Sr_2MgSi_2O_7$: Eu^{2+}, Dy^{3+} phosphor but also enhances the rate of solid state reaction, so as to achieve the purpose of reducing the sintering temperature. The photoluminescence performance of the sample with a Si/Sr ratio of 1.1 sintered at 1350 °C is the highest, followed by that of the sample sintered at 1400 °C with a Si/Sr ratio of 1.0. Notably, the photoluminescence properties of the Si/Sr ratio of 1.3 sample sintered at 1300 °C are comparable to those of the Si/Sr ratio of 1.0 sample sintered at 1400 °C. However, in terms of afterglow properties, the former exhibits an enhancement by a factor of 3.5 compared to the latter. This finding suggests that strategically increasing the Si/Sr ratio can reduce the sintering temperature by 100 °C while maintaining or even enhancing the luminescence and afterglow properties of the samples. Additionally, the electronic structures of the $Sr_2MgSi_2O_7$ host, the doped luminescence center Eu, the oxygen vacancies and the co-doped activator Dy have been methodically investigated through first-principles calculations. By integrating the findings on the distribution of the dopants and defects levels, we predict and propose the photoluminescence and afterglow mechanisms of $Sr_2MgSi_2O_7$: Eu^{2+}, Dy^{3+}. These studies suggest an efficient, cheap and energy-saving strategy for the preparation of $Sr_2MgSi_2O_7$: Eu^{2+}, Dy^{3+} long afterglow phosphor, and reveal the roles of oxygen vacancies and co-doped Dy in the afterglow luminescence.

Keywords $Sr_2MgSi_2O_7$, Persistent luminescence, Optimizing synthesis, First-principles calculation, Electron traps

Long afterglow phosphors are a special kind of environment-friendly light source materials, ones not only have excellent photoluminescence performance, but also can store luminous energy from UV light, lamplight or sunlight and then release the energy slowly. The development of afterglow phosphors has been experienced from sulfides to aluminates to silicates. Long lasting phosphorescent silicates have been widely investigated for their excellent water resistance and good chemical stability[1,2], among them $Sr_2MgSi_2O_7$: Eu^{2+}, Dy^{3+} is presumably the best known persistent luminescent silicate, and its brightness and lifetime of the afterglow overshadows that of most silicates[3–5].

Different methods were investigated to obtain $Sr_2MgSi_2O_7$: Eu^{2+}, Dy^{3+} phosphor, such as solid state reactions[6], sol-gel technique[7] and microwave[8]. Photoluminescence and afterglow properties are also depended on the synthetic methods. The high temperature solid state reaction process, which is a conventional preparation technique, is commonly used in industrial production because of its simple technology, perfect crystalline quality, less surface defects, high luminescence brightness and long persistent duration. But some problems still exist such as high calcination temperature, long maintaining time and impurity phases. Solid state reaction

[1]College of Electrical Engineering, Henan University of Technology, Zhengzhou 450001, China. [2]Department of Network Security, Henan Police College, Zhengzhou 450046, China. [3]Spallation Neutron Source Science Center, Dongguan 523803, China. [4]Key Laboratory of Functional Composite Materials of Guizhou Province, College of Big Data and Information Engineering, Guizhou University, Guiyang 550025, China. [5]Anqiu Qingyun Bilingual School, Weifang, China. ✉email: chizhang@haut.edu.cn; cydeng@gzu.edu.cn; 104752170073@vip.henu.edu.cn

often requires high sintering temperature. This is because atoms in the solid need enough energy to diffuse and migrate. The atoms are constantly vibrating around their equilibrium positions in solids, and the amplitude of this vibration will increase as the temperature rises. The energy obtained from the external environment will induce the release of atoms, thereby facilitating their diffusion and migration within the solid. The higher the temperature, the greater the proportion of diffuse atoms, thus promoting solid state reactions. In our research, we have found that a sintering temperature of at least 1400 °C is required to synthesize $Sr_2MgSi_2O_7$ with good performance without adding flux. In addition, the $Sr_3MgSi_2O_8$ phase is commonly observed as an impurity phase in the $Sr_2MgSi_2O_7$ sample[9–11], which will adversely affect the investigation of the performance of $Sr_2MgSi_2O_7$. According to coordination polyhedron regulation of anion, silicium-oxygen tetrahedron $[SiO_4]^{4-}$ is basic structural unit of silicate crystals. Therefore, the formation of $Sr_3MgSi_2O_8$ phase with isolated orthosilicate anions $[SiO_4]^{4-}$ is more readily achieved than $Sr_2MgSi_2O_7$ phase with isolated double tetrahedra $[Si_2O_7]^{6-}$. Consequently, the conventional solid state reaction synthesis of $Sr_2MgSi_2O_7$: Eu^{2+}, Dy^{3+} phosphors faces two critical challenges that limit their industrial implementation: (1) the excessively high sintering temperatures required for phase formation result in substantial energy consumption, and (2) the formation of impurity phases can significantly deteriorate the luminescence and afterglow performance of the material.

Silica, as a crucial raw material for solid state reaction of silicate phosphors, significantly influences the crystalline structure, luminescence and afterglow properties of the resulting materials. Y. Li et al. systematically investigated the effects of non-stoichiometry on photoluminescence and afterglow properties of $Sr_2MgSi_nO_{3+2n}$: Eu^{2+}, Dy^{3+} ($1.8 \le n \le 2.2$) by solid-state reaction[12]. Their findings demonstrate that the samples with SiO_2 excess possess better crystallinity and larger, and both photoluminescence intensity and afterglow performance have also improved. H. Y. Jiao et al. synthesized phosphors of $Ca_{1.86}Al_2Si_{1+y}O_{7+2y}$: $0.14Eu^{3+}$ ($0 \le y \le 0.3$) with excess SiO_2, and confirmed that the photoluminescence intensity of the obtained phosphors is fairly enhanced by excessive SiO_2[13]. C. Deng et al. reported that bridging oxygen can be formed relatively easily in the $Ca_2MgSi_2O_7$: Eu^{2+}, Dy^{3+} phosphors with the increase of silicon-calcium stoichiometric ratio. This increases the formation of the $Ca_2MgSi_2O_7$ and $CaMgSi_2O_6$ phases while inhibiting the generation of impurity phase $Ca_3MgSi_2O_8$[14]. In summary, the addition of an appropriate amount of silica during the high-temperature solid-state reaction process for synthesizing silicate phosphors containing double tetrahedra ($[Si_2O_7]^{6-}$) not only enhances the luminescence and afterglow properties of the phosphors but also effectively prevents the formation of impurity phases with isolated orthosilicate anions ($[SiO_4]^{4-}$), such as $Ca_3MgSi_2O_8$. However, the effects of excessive silica on the synthesis process of silicate phosphors, as well as the underlying mechanisms responsible for the observed improvements in luminescence and afterglow properties, still require further investigation and discussion.

In the present work, $Sr_{1.94}MgSi_2O_7$: $Eu^{2+}_{0.01}$, $Dy^{3+}_{0.05}$ phosphors with different Si/Sr ratios were successfully prepared by solid state reaction method at different sintering temperature. Through a systematic investigation of the effects of varying the Si/Sr ratio at different sintering temperatures on the phases, crystallinity, grain size, solid state diffusion, reaction process, photoluminescence and afterglow properties of the $Sr_{1.94}MgSi_2O_7$: $Eu^{2+}_{0.01}$, $Dy^{3+}_{0.05}$ phosphors, it was confirmed that increasing the Si/Sr ratio in the $Sr_2MgSi_2O_7$ host effectively enhances the rate of solid state reaction, which has the same effect as increasing the sintering temperature. Therefore, the $Sr_2MgSi_2O_7$: Eu^{2+}, Dy^{3+} phosphors with excellent photoluminescence and afterglow properties can be obtained by optimizing the Si/Sr ratio, and the sintering temperature can be reduced. In addition, despite numerous studies on the mechanism[15–17], the afterglow mechanism of $Sr_2MgSi_2O_7$: Eu^{2+}, Dy^{3+} remains a subject of controversy. The electronic structures of $Sr_2MgSi_2O_7$ host, dopants and oxygen vacancies (V_O and V_O^{2+}) were obtained based on first-principles calculation. This theoretical investigation provides valuable support for elucidating the roles of dopant Dy and oxygen vacancies in long afterglow luminescence. The research results offer a valuable reference for the prediction of the afterglow luminescence mechanism of $Sr_2MgSi_2O_7$: Eu^{2+}, Dy^{3+}. These studies may have contribution to decrease the production cost, promote energy saving and improve industrial production efficiency.

Methods

Experimental methods

The samples $Sr_{1.94}MgSi_2O_7$: $Eu^{2+}_{0.01}$, $Dy^{3+}_{0.05}$ with different SiO_2 addition amount were synthesized by solid state reaction method at different temperature (1250 °C, 1300 °C, 1350 °C and 1400 °C), and the different amounts of SiO_2 are measured by molar ratios of Si/Sr = 1, 1.1, 1.2, 1.3 and 1.4, respectively. solid powders $SrCO_3$ (AR), MgO (AR), SiO_2 (3 N), Eu_2O_3 (4 N) and Dy_2O_3 (3 N) were raw materials. The raw materials weighed according to stoichiometric ratio were mixed thoroughly in an agate mortar and pre-sintered at 800 °C for 2 h in air. The pre-sintering powders were ground again, pressed into tablets and sintered at different temperature (1250 °C, 1300 °C, 1350 °C and 1400 °C) for 4 h under a reducing atmosphere of carbon monoxide. However, the samples sintered at 1400 °C with Si/Sr ratios greater than 1 melted completely, thus only the sample Si/Sr = 1 (sintered at 1400 °C) was retained.

To determine the crystalline phases of all samples, a Rigaku Smartlab X-ray diffractometer (XRD) with Cu Kα radiation was utilized. The scan range (2θ) was from 10 to 80°. The morphologies and microstructures of samples were observed by Scanning Electron Microscope (SEM). Room temperature emission and excitation spectra were measured on a HORIBA FluoroMax®-4 spectrofluorometer. Afterglow decay curves were recorded on the same spectrofluorometer, and all samples were irradiated by a 365 nm ultraviolet lamp for 30 min before the afterglow performance measurements.

Computational details and modeling

In order to thoroughly investigate the afterglow mechanism of long afterglow phosphors $Sr_2MgSi_2O_7$: Eu^{2+}, Dy^{3+}, the Vienna ab initio simulation package (VASP)[18,19] was employed for the first-principles calculations based on density functional theory (DFT) to study the electronic properties of $Sr_2MgSi_2O_7$ and the dopants and defects

in it. The exchange-correlation functional is described by the generalized gradient approximation (GGA)[20] with the Perdew-Burke-Ernzerhof (PBE). The valence electron configurations in the calculation are Sr($4s^2 4p^6 5s^2$), Mg($2p^6 3s^2$), Si($3s^2 3p^2$), O($2s^2 2p^4$), Eu($4f^7 5d^0 6s^2$), Dy($4f^{10} 5d^0 6s^2$), and the projector augmented wave (PAW) is used to describe the interaction between valence electrons and their respective nuclei. The modified Becke Johnson (mBJ) exchange-correlation potential is employed to modify the issue of underestimation in band gap[21], thereby enhancing the congruity between calculated results and experimental data.

The crystal structure of $Sr_2MgSi_2O_7$ is depicted in Fig. 1a. When constructing the doping and defect calculation models, the unit cell of $Sr_2MgSi_2O_7$ was initially expanded into a 1 × 1 × 2 supercell. The oxygen vacancy model of $Sr_2MgSi_2O_7$ was obtained by removing an O atom from the supercell, as shown in Fig. 1b. Since the ionic radii of Eu^{2+} (0.125 nm) and Dy^{3+} (0.1027 nm) are similar to the ionic radii of Sr^{2+} (0.126 nm) in $Sr_2MgSi_2O_7$ crystal, the doped Eu^{2+} or Dy^{3+} ions enter the host to replace the lattice sites of Sr^{2+} ions. By substituting one Sr atom in the supercell with a Eu or Dy atom, the doping models of $Sr_{1.875}Eu_{0.125}MgSi_2O_7$ and $Sr_{1.875}Dy_{0.125}MgSi_2O_7$ were obtained, as illustrated in Fig. 1c and d, respectively.

Results and discussion

Phase identification and morphology

The XRD patterns of samples (Si/Sr = 1, 1.1, 1.2, 1.3 and 1.4) sintered at 1250 °C, 1300 °C and 1350 °C are shown in Fig. 2a, b and c, respectively. Figure 2d shows the XRD pattern of Si/Sr = 1 sample sintered at 1400 °C. The major diffraction peaks of all samples can be indexed to a tetragonal $Sr_2MgSi_2O_7$ phase according to JCPDS Cards 75-1736. $Sr_2MgSi_2O_7$ is the melilite-type crystal structure, which belongs to tetragonal crystallography with space group $P\text{-}42_1m$, and the corresponding lattice parameters are a = b = 7.9957 Å, c = 5.1521 Å, α = β = γ = 90°. In the XRD patterns of all Si/Sr = 1 samples sintered at 1250 °C to 1400 °C and Si/Sr = 1.1 sample sintered at 1250 °C, two diffraction peaks located approximately at 31.4° and 32.2° (indicated by "•") are not attributed to $Sr_2MgSi_2O_7$ phase. Based on the phase analysis, these two diffraction peaks matched well with the standard card of $Sr_3MgSi_2O_8$ (JCPDS Cards 10–0075), which is consistent with the reports in literatures[22–24]. Thus, the impurity phase $Sr_3MgSi_2O_8$ exists in these samples. With the continuous increase of Si/Sr ratio, $Sr_2MgSi_2O_7$

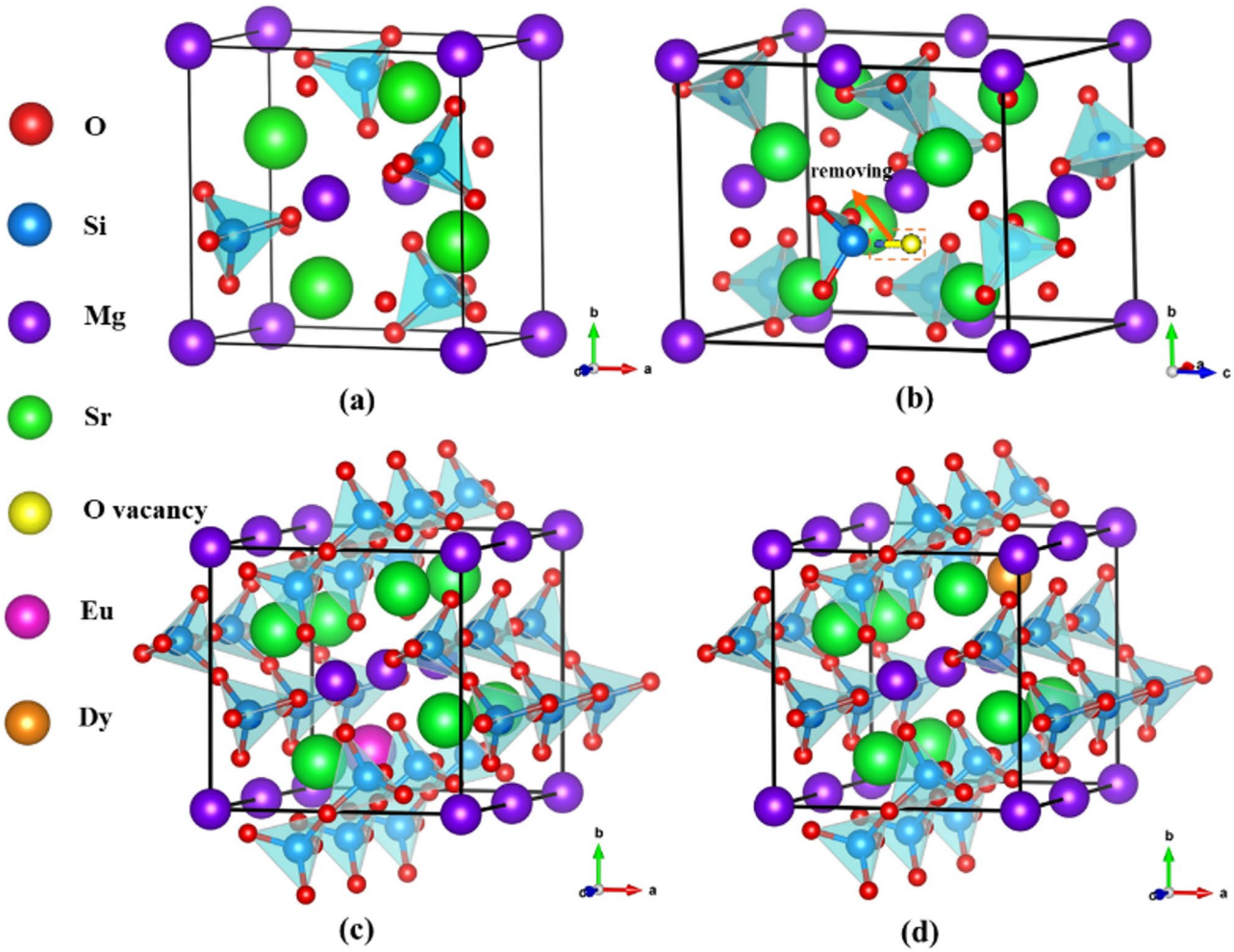

Fig. 1. Crystal structure of $Sr_2MgSi_2O_7$ unit cell (**a**), $Sr_2MgSi_2O_7$ with oxygen vacancy (**b**), $Sr_{1.875}Eu_{0.125}MgSi_2O_7$ (**c**) and $Sr_{1.875}Dy_{0.125}MgSi_2O_7$ (**d**), respectively.

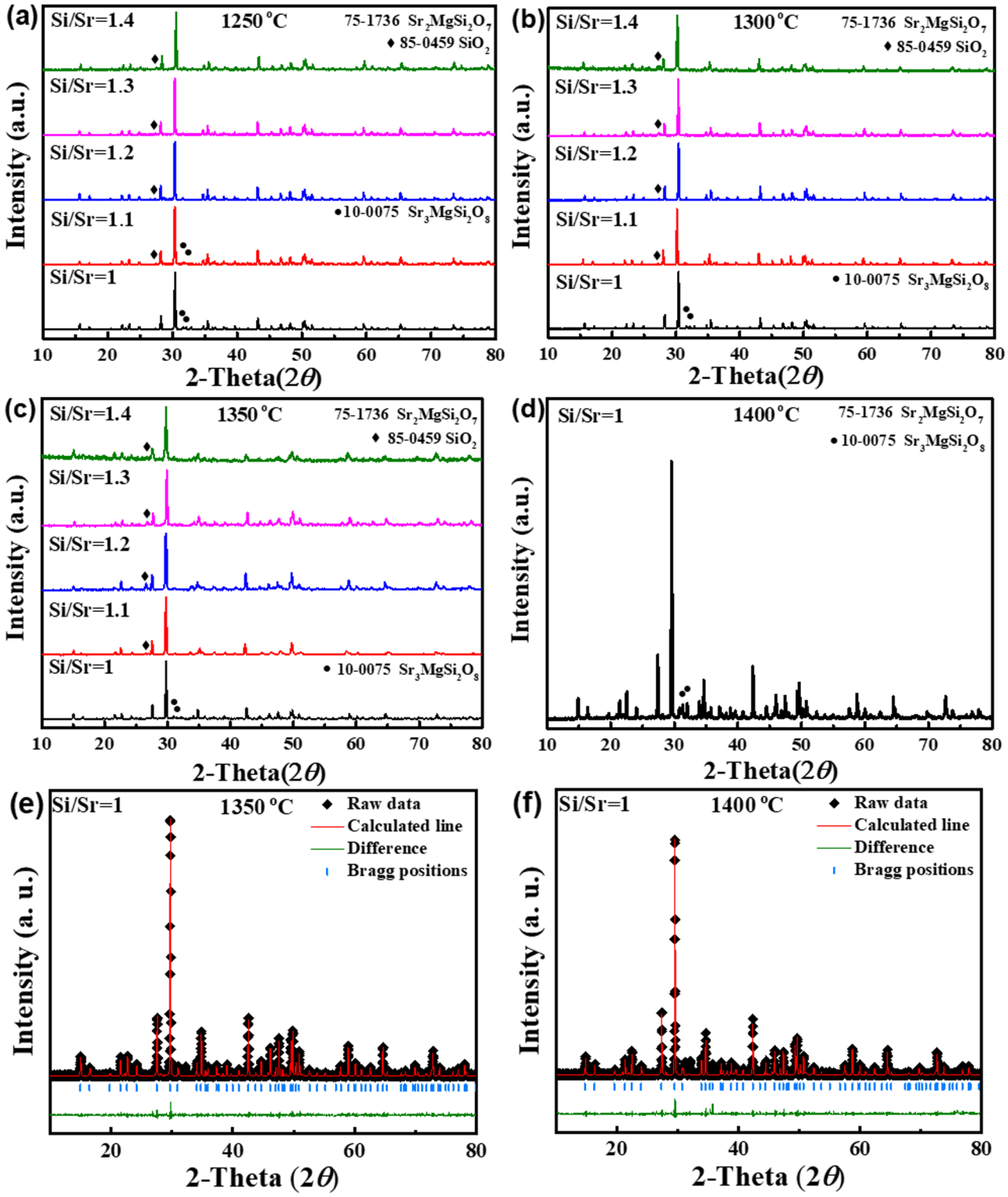

Fig. 2. (**a**–**d**) XRD patterns of $Sr_{1.94}MgSi_2O_7$: $Eu^{2+}_{0.01}$, $Dy^{3+}_{0.05}$ phosphors with different silicium-strontium ratios (Si/Sr = 1, 1.1, 1.2, 1.3 and 1.4), and the sintering temperatures are (**a**) 1250 °C, (**b**) 1300 °C, (**c**) 1350 °C and (**d**) 1400 °C, respectively. (**e**–**f**), (**b**–**d**) Rietveld refinement of the $Sr_{1.94}MgSi_2O_7$: $Eu^{2+}_{0.01}$, $Dy^{3+}_{0.05}$ (Si/Sr = 1) phosphors sintered at 1350 °C and 1400 °C, respectively.

phase (JCPDS Cards 75-1736) containing a small amount of excessive SiO_2 (JCPDS Cards 85–0459, indicated by "◆") is obtained, as shown in Fig. 2a, b and c.

As depicted in the XRD patterns of samples with Si/Sr = 1 (Fig. 2), it can be observed that impurity phase $Sr_3MgSi_2O_8$ does not disappear as the sintering temperature rises. In the crystal structure of $Sr_3MgSi_2O_8$, the

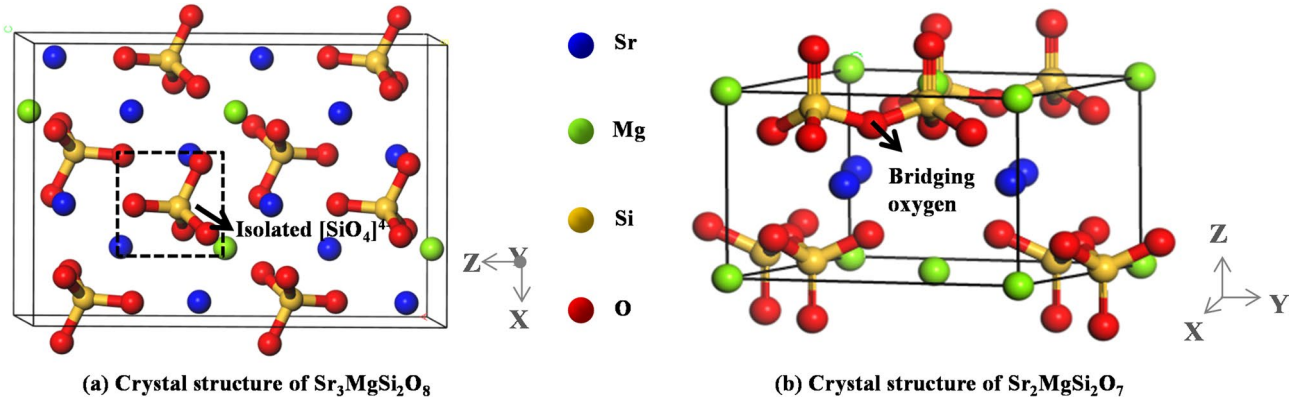

Fig. 3. Crystal structures of $Sr_3MgSi_2O_8$ (**a**) and $Sr_2MgSi_2O_7$ (**b**).

Temp.	Si/Sr	a	b	c	Volume (a*b*c)
1250 °C	1	8.00	8.00	5.16	330.24
	1.1	8.00	8.00	5.16	330.24
	1.2	8.01	8.01	5.16	331.07
	1.3	8.01	8.01	5.16	331.07
	1.4	7.99	7.99	5.15	328.78
1300 °C	1	8.01	8.01	5.16	331.07
	1.1	8.03	8.03	5.18	334.01
	1.2	8.00	8.00	5.16	330.24
	1.3	8.01	8.01	5.17	331.71
	1.4	8.01	8.01	5.18	332.35
1350 °C	1	8.00	8.00	5.15	329.60
	1.1	7.99	7.99	5.13	327.50
	1.2	7.99	7.99	5.13	327.50
	1.3	7.98	7.98	5.14	327.32
	1.4	7.98	7.98	5.14	327.32
1400 °C	1	7.99	7.99	5.13	327.50
Calculation	1	8.08	8.08	5.22	340.80

Table 1. Variation of lattice parameters for samples with various Si/Sr ratios at different sintering temperatures.

ratio of silicon atoms to oxygen atoms is 1:4, so silicon-oxygen tetrahedron occurs as isolated $[SiO_4]^{4-}$ center (Fig. 3 a). Figure 3b shows the crystal structure of $Sr_2MgSi_2O_7$. Two tetrahedra are joined together by a bridging oxygen, and a double tetrahedra structure $[Si_2O_7]^{6-}$ is formed in the $Sr_2MgSi_2O_7$ crystal structure. To eliminate the impurity phase $Sr_3MgSi_2O_8$, it is imperative to facilitate the formation of bridge oxygen. In a reducing atmosphere, the Si/O ratio is enhanced as the silicon contents increase, which is beneficial to the formation of bridging oxygen in the $Sr_2MgSi_2O_7$. Consequently, the impurity phase $Sr_3MgSi_2O_8$ is eliminated with the increase of Si/Sr ratio.

The lattice parameters of all samples and $Sr_2MgSi_2O_7$ calculation model by structure optimization are listed in Table 1. The lattice parameters basically expand first and then reduce with the increase of sintering temperature or Si/Sr ratio. The expansion of the lattice parameters caused by sintering temperature or Si/Sr ratio may be related to the high temperature lattice expansion and the introduction of excess Si atoms in the interstitial positions, respectively. However, as the sintering temperature or Si/Sr ratio continues to increase, the smaller lattice parameters may be caused by the increase of vacancies in the samples which will affect the afterglow performances. The lattice parameters of $Sr_2MgSi_2O_7$ calculation model after structure optimization closely resemble those of the experimental samples, indicating that the geometrically optimized crystal structure is highly consistent with the experimental samples.

The SEM images of Si/Sr = 1, 1.1, 1.3 and 1.4 samples sintered at 1350 °C are shown in Fig. 4a, b, c and d, respectively, and the diagrammatic sketch of sintering process are shown in Fig. 4e–h. The particles in the unsintered tablets are only in point contact or not in contact at all, as depicted in Fig. 4e. At the initial sintering stage (Fig. 4f), the gas is expelled from the tablets, particles begin to rearrange and gather, and the particles of diffusion phases SrO and MgO are likely to surround SiO_2. There is still point contact between the particles, but the number of contact points increases. Mass transfer is happened at the contact point with the increasing

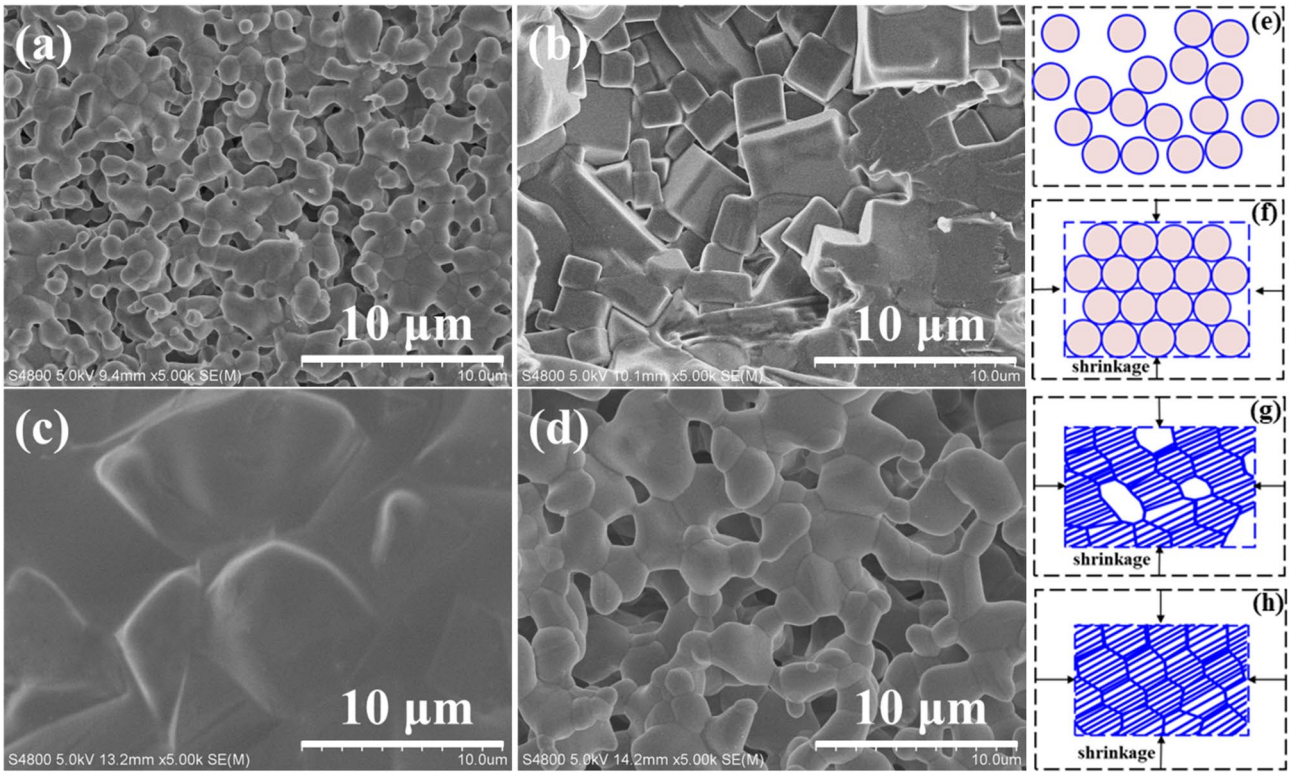

Fig. 4. SEM images of (**a**) Si/Sr = 1, (**b**) Si/Sr = 1.1, (**c**) Si/Sr = 1.3 and (**d**) Si/Sr = 1.4 samples sintered at 1350 °C, and diagrammatic sketch of sintering process (**e**–**h**).

sintering temperature or holding time. The contact surface is gradually expanding and the grain boundary is formed. As the mass transfer continues, the area of grain boundary increases, porosity decreases, volume shrinks, and the new crystal phase is formed gradually (Fig. 4g). After that, the grains grow unceasingly, and the pores are expelled gradually with the movement of the grain boundary. Ultimately, the dense polycrystals are synthesized as shown in Fig. 4h.

The SEM image of Si/Sr = 1 sample sintered at 1350 °C shows a comparatively looser structure. There are many independent or connected pores in the Si/Sr = 1 sample. The loose porous crystal structure in Fig. 4a is similar to Fig. 4g, which illustrates the sample with many lattice defects is still in the stage of grain growth. This indicates that at Si/Sr = 1, a sintering temperature of 1350 °C only leads to the formation of $Sr_2MgSi_2O_7$ crystal phase, while the reaction conditions fail to expel pores and achieve dense crystal. As shown in Fig. 4b, the SEM image of Si/Sr = 1.1 sample sintered at 1350 °C is similar to Fig. 4h. The sample has tetragonal crystal grains with uniform distribution, regular morphology and high denseness. When sintering temperature, holding time and atmosphere remain unchanged, the product can be changed from a loose porous crystal structure (Fig. 4a, representing the stage of grain growth) to the ideal dense polycrystals (Fig. 4b) by solely increasing the Si/Sr ratio. It is shown that the increase of Si/Sr ratio can effectively promote the diffusion mass transfer during solid state reaction and improve the rate of solid state reaction, which achieves the similar effect as raising the sintering temperature or prolonging the holding time.

In addition, the abnormal growth of grains with larger size caused by secondary recrystallization can be observed in the SEM image of Si/Sr = 1.3 sample (Fig. 4c), which is typically attributed to the rapid movement of grain boundaries resulting from excessive diffusion coefficient in solid state reaction. As depicted in Fig. 4d, when the Si/Sr ratio rises to 1.4, along with the abnormal grain growth phenomenon, an abundance of pores is also observed. The formation of this porous structure is caused by the over-rapid diffusion rate. Since the rate movement of grain boundary is obviously higher than that of pores during the secondary recrystallization, the grain boundaries may over the pores and these pores are hard to be expelled by bulk diffusion. The secondary recrystallization of samples Si/Sr = 1.3 and Si/Sr = 1.4 sintered at 1350 °C also reveals that the grain growth rate escalates with the Si/Sr ratio. This finding further substantiates the conclusion that an increased Si/Sr ratio can effectively enhance the rate of solid state reaction, and its effect is similar to the increase of sintering temperature. The melting of all samples with excess Si content at 1400 °C also illustrates that increasing both the Si/Sr ratio and the sintering temperature results in similar enhancements of solid state reaction rate.

The solid state reaction rate is accelerated with the increase of the Si/Sr ratio, which can also be explained by solid state diffusion and reaction process. In the multicomponent reaction system for synthesizing $Sr_2MgSi_2O_7$, the solid state reaction rate depends on the slower diffusion particles. The highly charged ions such as Si^{4+} are less free to migrate than divalent ions[25]. Thus, the cations Sr^{2+} and Mg^{2+} are the migrating ions, and the reaction rate depends very much on the diffusion of Si^{4+} ions. The concentration of Si^{4+} increases with the

augmentation of silicon content in raw materials, which is beneficial to improving the contact opportunity of reactants and promoting the diffusion of Si^{4+} ions, thereby leading to an increased rate of solid state reaction. Based on principles of solid state reaction and crystallography of silicates, the reaction process is depicted in equations in Fig. 5. In the solid state reaction of $Sr_2MgSi_2O_7$, the synthesis of both the initial products and the crucial intermediate product necessitate SiO_2 participation. Therefore, enhancing the quantity of SiO_2 addition in the raw material can effectively enhance the areas of reaction interface, thereby significantly augmenting the rate of solid state reaction.

Photoluminescence properties

Figure 6a shows the photoluminescence excitation spectra of all samples, and all excitation spectra are monitored by 467 nm. A broad excitation band is exhibited in each excitation spectrum and the excitation peak is located at about 397 nm. However, two other excitation bands centered at about 358 nm and 370 nm are shown in excitation spectra of all Si/Sr = 1 samples and Si/Sr = 1.1 sample sintered at 1250 °C, which corresponds to the excitation spectrum of $Sr_3MgSi_2O_8$: Eu^{2+} reported in literature[26]. According to the results of phase analysis, the diffraction peaks corresponding to the $Sr_3MgSi_2O_8$ phase of these samples were also identified in the XRD patterns. Consequently, the abnormal excitation peaks observed in these samples are attributed to the excitation of impurity phase $Sr_3MgSi_2O_8$: Eu^{2+}.

Emission spectra (λ_{ex} = 397 nm) for all samples are shown in Fig. 6b. There is only one 467 nm emission band in the emission spectrum of each sample. All emission bands are attributed to the $4f^7$-$4f^65d^1$ typical transition of Eu^{2+}[27]. No special emission peaks of Dy^{3+} and Eu^{3+} are observed in the emission spectra[28,29]. The emission peak of $Sr_3MgSi_2O_8$: Eu^{2+} is located near 457 nm[26], which is close to the position of the emission peak of $Sr_2MgSi_2O_7$: Eu^{2+}. Therefore, no obvious emission peak of impurity phase $Sr_3MgSi_2O_8$: Eu^{2+} is found in the emission spectra of all Si/Sr = 1 samples and Si/Sr = 1.1 sample sintered at 1250 °C. Additionally, since the impurity phase SiO_2 does not exhibit a remarkable emission, it does not influence the position of the emission peak of the major phase $Sr_2MgSi_2O_7$: Eu^{2+}. However, it may have a slight impact on the photoluminescent intensity of the samples[30].

Figure 7 exhibits the dependence of the photoluminescence intensity on sintering temperature. As shown in Figs. 6b and 7, at the same sintering temperature, the photoluminescence intensity of all samples changes regularly with the Si/Sr ratio. With the increase of Si/Sr ratio, the photoluminescence intensity of samples gradually increases at 1250 °C, when sintering temperature is raised to 1300–1350 °C, the photoluminescence intensity first increases and then decreases. When the sintering temperatures are set at 1250 °C, 1300 °C and 1350 °C, the samples with the optimum photoluminescence performance are Si/Sr = 1.4, Si/Sr = 1.3 and Si/Sr = 1.1, respectively. The property of Si/Sr = 1.4 sample sintered at 1250 °C is almost twice that of Si/Sr = 1 sample sintered at 1300 °C, and is similar to the performance of Si/Sr = 1 sample sintered at 1350 °C. The photoluminescence intensity of Si/Sr = 1.3 sample sintered at 1300 °C is almost the same as Si/Sr = 1 sample sintered at 1400 °C, and the photoluminescence performance of Si/Sr = 1.1 sample sintered at 1350 °C is the best of all. These descriptions of photoluminescence properties provide three results: (1) The appropriate increase of Si/Sr ratio can improve the photoluminescence property at the same sintering temperature. (2) Properly enhancing the Si/Sr ratio can reduce the sintering temperature by 100 °C and maintain good photoluminescence performance. (3) To obtain samples with excellent photoluminescence performances, the higher the sintering temperature is, the smaller the required Si/Sr ratio is.

The relationship between photoluminescence intensity and sintering temperature of samples with different Si/Sr ratios is shown on the right side of Fig. 7. The photoluminescence intensities of Si/Sr = 1, 1.1 and 1.2 samples increase steadily as sintering temperature increases, but the variation curve of Si/Sr = 1.2 tends to be gentle when the temperature rises from 1300 °C to 1350 °C. Nevertheless, the intensity of Si/Sr = 1.3 sample reaches the peak at 1300 °C and then starts to fall, and the intensity of Si/Sr = 1.4 sample falls off precipitously with the increase

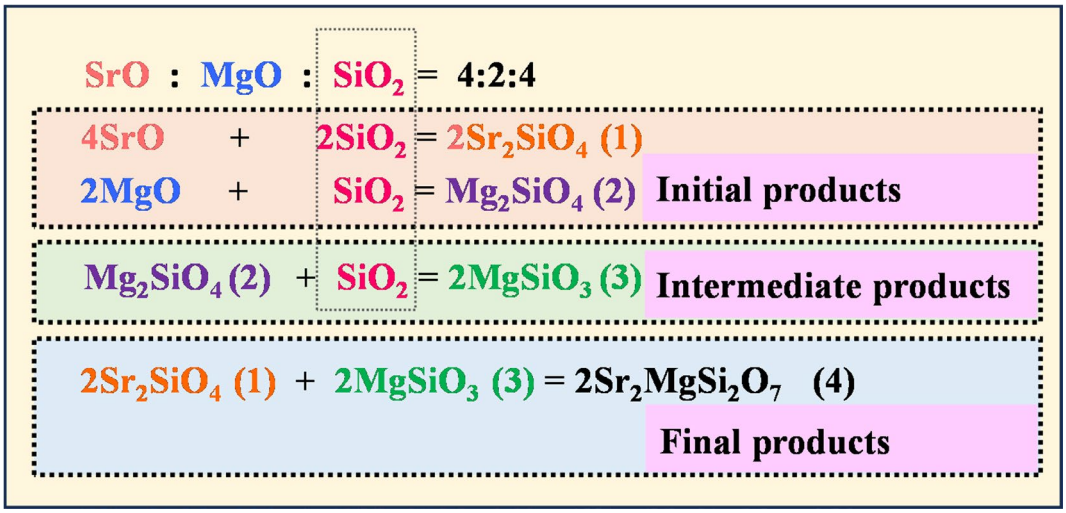

Fig. 5. Solid state reaction process of $Sr_2MgSi_2O_7$.

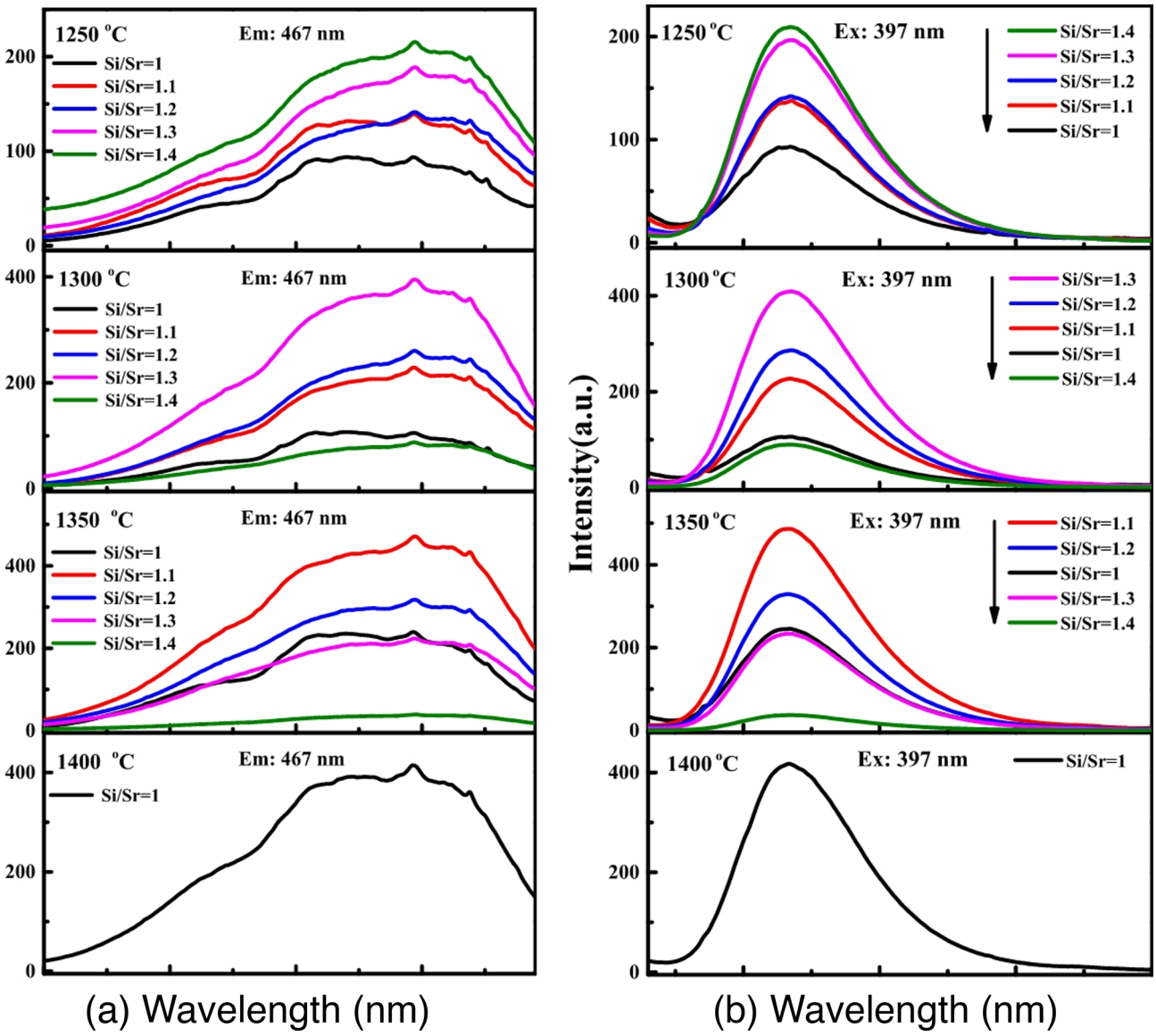

Fig. 6. Excitation (**a**) and emission (**b**) spectra of $Sr_{1.94}MgSi_2O_7$: $Eu^{2+}_{0.01}$, $Dy^{3+}_{0.05}$ phosphors with different silicium-strontium ratios (Si/Sr = 1, 1.1, 1.2, 1.3 and 1.4).

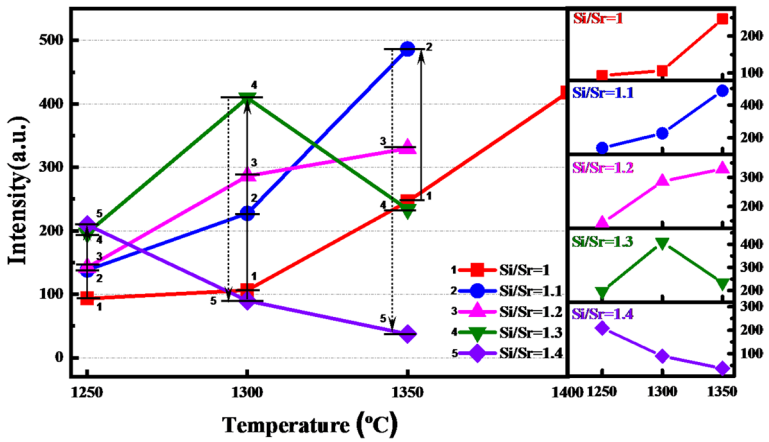

Fig. 7. Dependence of the photoluminescence intensity on sintering temperature.

of sintering temperature. The regularity of the above trend graph further proves that the photoluminescence performance deteriorates when the temperature and the Si/Sr ratio increase simultaneously.

The photoluminescence properties of samples are improved by increasing sintering temperature or adding Si/Sr ratio within an appropriate range. However, a higher Si/Sr ratio leads to a decrease in the required sintering temperature. On the one hand, sintering temperature is an important factor for the solid state reaction. Diffusion is often the only way of mass transfer in solids. Generally, the higher the sintering temperature is, the faster the rate of atom diffusion is. The enhanced diffusion rate can facilitate activator and auxiliary activator entering into the appropriate lattice sites and be beneficial to expelling the pores in the materials, so the effective density of doped ions and sintered density are improved by raising sintering temperature. On the other hand, raising the proportion of silica in reactants facilitates the sufficient dispersion of SrO and MgO particles around SiO_2 at the rearrangement stage, which enlarges the areas of reaction interface and diffusion boundary. Therefore, the increase of Si/Sr ratio can also enhance the rate of solid state reaction and facilitate the activator entering the crystal lattice. In conclusion, whether sintering temperature or Si/Sr ratio increases, the rate of solid state reaction can be improved. Obviously, increasing the Si/Sr ratio yields a similar effect to raising the sintering temperature, thereby enhancing the Si/Sr ratio can reduce the sintering temperature.

In addition, the photoluminescence performances of the samples are also affected by the crystallization properties. As the result of SEM analysis, Si/Sr = 1.1 sample sintered at 1350 °C has very regular hexahedron crystal morphology with well crystallization, so it has the best photoluminescence performance. The large grains caused by abnormal grain growth appear in SEM image of Si/Sr = 1.3 sample sintered at 1350 °C and result in poor photoluminescence performance. The poor crystallinity and looser structure also lead to the poor photoluminescence property of Si/Sr = 1.4 sample sintered at 1350 °C. Thus, the optimization of sintering temperature and Si/Sr ratio is crucial for controlling normal grain growth in order to achieve ideal polycrystalline materials, thereby enhancing the photoluminescence performance.

Afterglow characteristics

The decay curves in Fig. 8a–d exhibit variations corresponding to the Si/Sr ratio, and the dependence of the initial brightness of the afterglow on sintering temperature is illustrated in Fig. 8e. As shown in Fig. 8a–d, afterglow properties of samples exhibit enhancement with the increasing of Si/Sr ratio. The afterglow properties of Si/Sr = 1.4 samples sintered at 1250 °C, 1300 °C and 1350 °C are enhanced about 42, 27 and 13 times, respectively when compared to the Si/Sr = 1 samples sintered at the same temperature. Although the photoluminescence properties of Si/Sr = 1.3 sample sintered at 1300 °C and Si/Sr = 1 sample sintered at 1400 °C are similar, the former

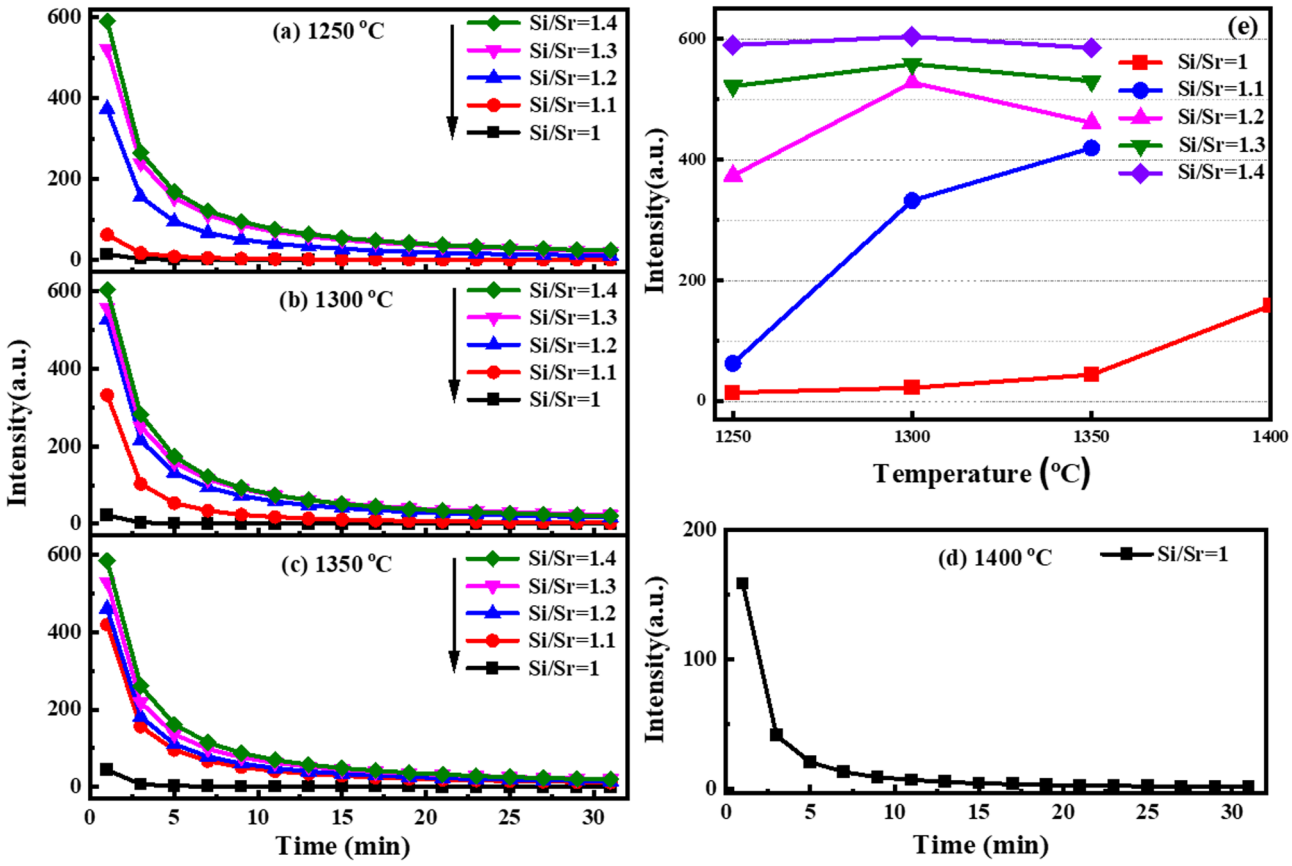

Fig. 8. (**a**–**d**) Afterglow decay curves of $Sr_{1.94}MgSi_2O_7$: $Eu^{2+}_{0.01}$, $Dy^{3+}_{0.05}$ phosphors with different silicium-strontium ratios and (**e**) dependence of the initial brightness of the afterglow on sintering temperature.

demonstrates the afterglow performance approximately 3.5 times greater than that of the latter. Therefore, the good photoluminescence and afterglow properties $Sr_2MgSi_2O_7$: Eu^{2+}, Dy^{3+} phosphors can be obtained through adjustment of Si/Sr ratio, and the sintering temperature can be reduced by at least 100 °C. This is attributed to the fact that a high concentration of traps can enhance the afterglow performance, while the incorporation of excess SiO_2 is beneficial for improving trap density[12]. In previous literatures, both Dy^{3+} ions and oxygen vacancies are important electron traps[31–36]. The doped Dy^{3+} ions not only introduce deeper electron traps but also act as electron donors. The higher Si/Sr ratio is conducive to raising the rate of atom diffusion and doping Dy^{3+} ions into the lattice, so the effective density of Dy^{3+} ions is improved by increasing Si/Sr ratio. Furthermore, when the samples were synthesized under a high temperature reducing atmosphere, the addition of excess SiO_2 resulted in an imbalanced Si/O ratio (oxygen deficiency), which favored the formation of oxygen vacancies. In consequence, the afterglow performance is ameliorated as the effective trap density increases.

As shown in Fig. 8a–e, afterglow properties of Si/Sr = 1 and Si/Sr = 1.1 samples are also improved as the sintering temperature increases. When the Si/Sr ratio is relatively low, the high sintering temperature can improve the crystallization capacity, facilitate Eu^{2+} and Dy^{3+} ions entering the crystal lattice and promote the formation of oxygen vacancies, thereby enhancing photoluminescence and afterglow properties. However, as the Si/Sr ratio increases (≥ 1.2), the differences in afterglow properties among samples sintered at different temperatures become less pronounced. This can be attributed to the fact that the effective trap density tends to be constant with the increased rate of solid state reaction. The afterglow properties of all Si/Sr = 1.4 samples are almost identical, surpassing the performance of Si/Sr = 1 sample sintered at 1400 °C by nearly 4 times. If only the afterglow performance is taken into consideration, the Si/Sr = 1.4 sample sintered at 1250 °C emerges as the optimal choice. This indicates that by increasing the Si/Sr ratio within an appropriate range, the $Sr_2MgSi_2O_7$: Eu^{2+}, Dy^{3+} phosphors with excellent afterglow performances can be synthesized at a lower sintering temperature. In addition, the afterglow properties of Si/Sr = 1.4 samples are hardly influenced by the crystallization as the sintering temperature rises, suggesting that the afterglow performance of $Sr_2MgSi_2O_7$: Eu^{2+}, Dy^{3+} sample is primarily determined by the trap levels.

Electronic structures

The computed energy band structure and total and partial density of states are shown in Fig. 9. As shown in Fig. 9a, The conduction band minimum (CBM) of host $Sr_2MgSi_2O_7$ is located at the high symmetry point G, while the valence band maximum (VBM) is situated at the point Z, which belongs to indirect band gap. The calculation results reveal that $Sr_2MgSi_2O_7$ is an insulator with band gap width of 6.88 eV, which closely matches the experimental value of 7.1 eV obtained by Tuomas Aitasalo et al. using UV-VUV synchrotron radiation[37]. Figure 9b illustrates the calculated energy band structure and density of states of Eu-doped $Sr_2MgSi_2O_7$. The Fermi level is positioned above the 4f levels of Eu within the band gap, indicating that the 4f levels within the band gap are occupied by electrons. The empty 5d levels of Eu are situated within the energy range of 0.61–4.42 eV above the bottom of the conduction band. Consequently, under the excitation of ultraviolet light, the

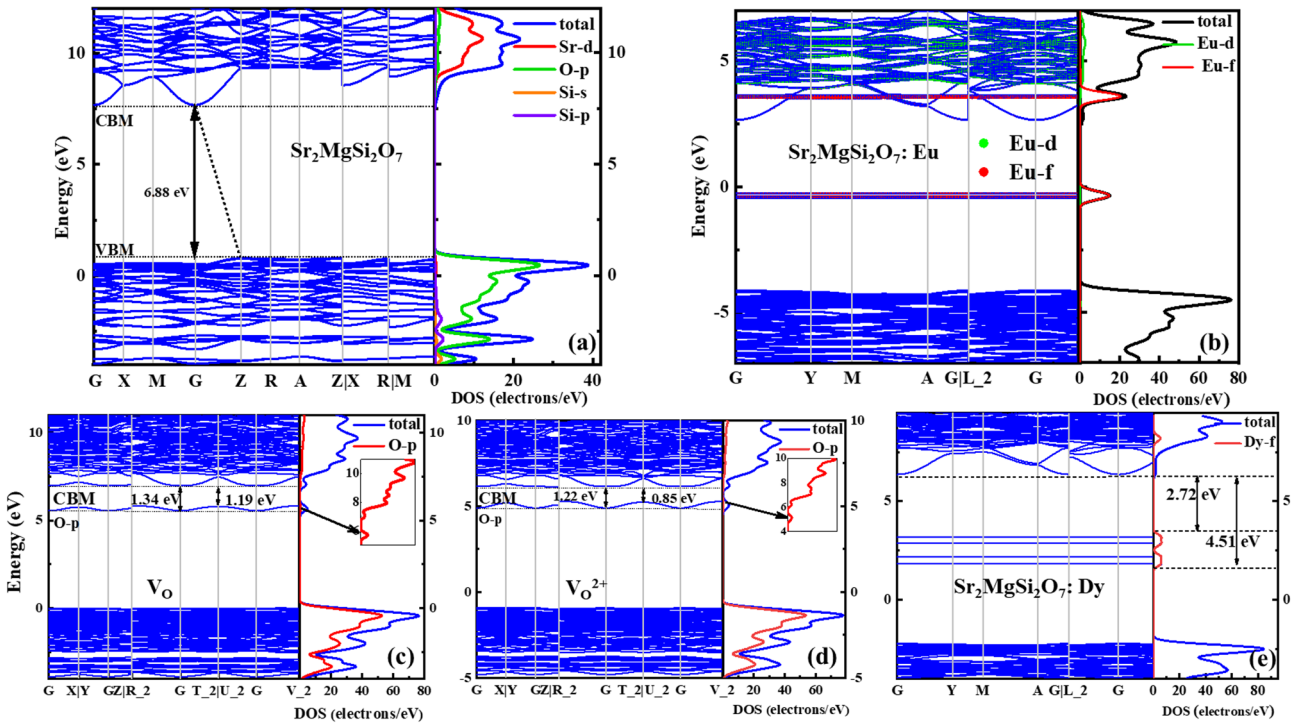

Fig. 9. Calculated energy band structure and density of states of (**a**) $Sr_2MgSi_2O_7$, (**b**) Eu-doped $Sr_2MgSi_2O_7$, (**c**–**d**) oxygen vacancies, (**e**) Dy-doped $Sr_2MgSi_2O_7$.

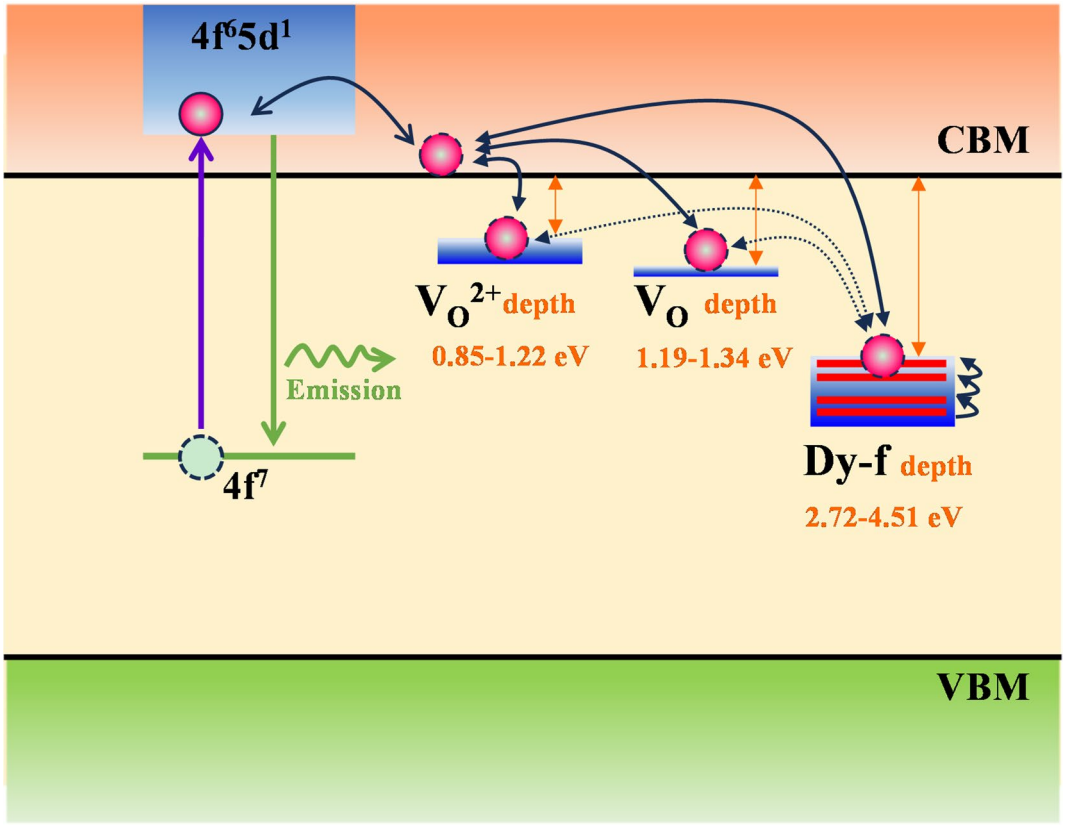

Fig. 10. Schematic diagram of afterglow mechanism of $Sr_2MgSi_2O_7$: Eu, Dy.

electron occupied the 4f levels of Eu absorb energy and transition to the unoccupied 5d levels. Subsequently, when the electrons in the 5d levels move back to the 4f levels, the characteristic emission of Eu occurs. Due to the fact that the 5d levels of Eu are located in the conduction band, the electrons excited to the 5d levels have the potential to enter the conduction band as free electrons. which may be captured by the defect energy levels in the crystal, and thus forming the phenomenon of afterglow.

We calculated the electronic structure of the oxygen vacancy (V_O) and the oxygen vacancy with two charges (V_O^{2+}) in $Sr_2MgSi_2O_7$, respectively. The corresponding energy band structures and density of states diagrams are presented in Fig. 9c and d, respectively. The defect energy levels of V_O and V_O^{2+} are located at 1.19–1.34 eV and 0.85–1.22 eV below the conduction band minimum, respectively, which are close to the bottom of the conductive band and easy to capture free electrons in the conductive band. Moreover, the electrons can easily escape from the trap levels by thermal activation and re-enter the conductive band. If they return to the 5d levels of Eu and transition back to the 4f levels, the afterglow is generated. Therefore, both oxygen vacancy (V_O) and charged oxygen vacancy (V_O^{2+}) are effective electron capture traps, playing a crucial role in the afterglow emission of $Sr_2MgSi_2O_7$: Eu, respectively.

In order to clarify the contribution of Dy in afterglow luminescence, the electronic structure of $Sr_2MgSi_2O_7$ doped with Dy was calculated. The obtained energy band structures and density of states are illustrated in Fig. 9e. The 4f levels of Dy within the forbidden band is distributed in the energy range of 2.72–4.51 eV below the conduction band, which is deeper than the trap levels generated by the oxygen vacancy, so the captured electrons are not easy to escape from the trap and return directly to the conduction band. The trapped electrons can undergo movements within the 4f levels of Dy until they reach the top of 4f trap level, or move to a nearby defect levels created by oxygen vacancy, and then move back to the conduction band. When they revert to the 5d levels of Eu, the afterglow may occur. Therefore, the trap levels generated by Dy play a key role in reducing the decay rate of afterglow and prolonging the luminescence time of afterglow.

Mechanism of afterglow luminescence

The schematic diagram illustrating the afterglow luminescence mechanism of $Sr_2MgSi_2O_7$: Eu, Dy is shown in Fig. 10. The emission spectrum of Eu in $Sr_2MgSi_2O_7$ is attributed to the characteristic emission of Eu^{2+} resulting from the transition between the $4f^65d^1$ excited state and the $4f^7$ ground state. The calculation results reveal that the 5d energy level of Eu is situated within the conduction band. When 4f electrons of Eu are excited and transition to the empty 5d levels, it is easy for them to enter the conduction band and become free electrons. These free electrons in the conduction band may be captured by the trap levels such as oxygen vacancies or the 4f levels of Dy if they move near them. The trap levels generated by oxygen vacancies are close to the conduction band bottom and belong to shallow trap levels. The electrons captured by them can easily overcome the potential

energy of the trap through thermal activation and return to the conduction band. Since the 5d levels of Eu is distributed above 0.61 eV from the conduction band bottom and has a small energy difference with the conduction band minimum. Free electrons, upon returning to the conduction band and approaching Eu, can re-enter the 5d levels of Eu, and then transition back to the 4f levels, thereby inducing the afterglow luminescence. The trap levels of Dy are relatively deep, so the captured electrons are not easy to return to the conduction band directly through thermally excitation. The electrons can be continuously transferred to the nearby 4f levels of Dy through thermal vibration until they reach the top of trap level, or move to the nearby trap levels of oxygen vacancy, and then they may further return to the conduction band, resulting in afterglow emission. The electrons captured by Dy 4f levels requires a relatively long process to return to the conduction band. Hence, the doping of Dy not only enhances the number of electron traps and captured electrons, but also effectively reduces the afterglow decay rate, prolongs the afterglow luminescence time and improve the afterglow performance.

Conclusions

In the process of solid state reaction to synthesize $Sr_2MgSi_2O_7$, increasing Si/Sr ratio can enhance the reaction rate, which is beneficial to the elimination of impurity phase $Sr_3MgSi_2O_8$ and promotes the formation of $Sr_2MgSi_2O_7$ phase. Additionally, it facilitates the growth of crystalline grain and the substitution of activator into the crystal lattice, exhibiting a similar effect to that achieved by raising sintering temperature. The photoluminescence performance of Si/Sr = 1.1 sample sintered at 1350 °C is the best of all. The photoluminescence intensity of Si/Sr = 1.3 sample sintered at 1300 °C is almost the same as Si/Sr = 1 sample sintered at 1400 °C, which is the second highest following the Si/Sr = 1.1 sample sintered at 1350 °C. Even with a reduction of 100 °C in the sintering temperature, the excellent luminescence properties can still be maintained. Therefore, the sample with good photoluminescence performance resulting from well crystallization and effective density of activators can be obtained through controlling Si/Sr ratio and sintering temperature within an appropriate range. However, the photoluminescence property may deteriorate due to the secondary crystallization when the sample has a large Si/Sr ratio and the sintering temperature is too high. The afterglow property of $Sr_{1.94}MgSi_2O_7$: $Eu^{2+}_{0.01}$, $Dy^{3+}_{0.05}$ mainly depends on the trap levels rather than the crystallization. The increase of the Si/Sr ratio is beneficial for improving trap density, resulting in significant improvements in the afterglow brightness, decay rate and luminescence time of $Sr_{1.94}MgSi_2O_7$: $Eu^{2+}_{0.01}$, $Dy^{3+}_{0.05}$. The calculation results reveal that the oxygen vacancies (V_O and V_O^{2+}) and Dy 4f levels introduce trap levels of different depths in the host of $Sr_2MgSi_2O_7$, which can effectively capture the electrons of Eu entering the conduction band. The addition of excess SiO_2 not only promotes the incorporation of Dy^{3+} into the lattice but also facilitates the formation of oxygen vacancies, thereby enhancing the effective trap density and improving the afterglow properties of the samples. In short, the research results of this work provide technical and theoretical guidance for optimizing the preparation process of $Sr_{1.94}MgSi_2O_7$: $Eu^{2+}_{0.01}$, $Dy^{3+}_{0.05}$, improving luminescence and afterglow performance, thus effectively promoting energy conservation and reducing production costs.

Data availability

The datasets used and/or analysed during the current study available from thecorresponding author on reasonablerequest.

Received: 18 September 2024; Accepted: 16 May 2025
Published online: 26 May 2025

References

1. Hai, O. et al. Exploration of long afterglow luminescence materials work as round-the-clock photocatalysts. *J. Alloys Compd.* **866**, 158752. https://doi.org/10.1016/j.jallcom (2021).
2. Zhang, J., Jin, Y., Wu, H., Chen, L. & Hu, Y. Giant enhancement of a long afterglow and optically stimulated luminescence phosphor $BaCaSiO_4$: Eu^{2+} via Pr^{3+} codoping for optical data storage. *J. Lumin.* **263**, 119971. https://doi.org/10.1016/j.jlumin.2023.119971 (2023).
3. Zou, L. et al. Enhanced long afterglow luminescence of $Sr_2MgSi_2O_7$: Eu^{2+}, Dy^{3+} by NH_4Cl. *Inorg. Chem. Commun.* **146**, 110151. https://doi.org/10.1016/j.inoche.2022.110151 (2022).
4. Van den Eeckhout, K., Smet, P. F. & Poelman, D. Persistent luminescence in Eu^{2+}-doped compounds: a review. *Materials* **3**, 2536–2566. https://doi.org/10.3390/ma3042536 (2010).
5. Yang, E. et al. Improved trap capability of shallow traps of $Sr_2MgSi_2O_7$: Eu^{2+}, Dy^{3+} through depositing Au nanoparticles. *J. Alloys Compd.* **858**, 157705. https://doi.org/10.1016/j.jallcom.2020.157705 (2021).
6. Wang, Y. et al. A new method for preparing cubic-shaped $Sr_2MgSi_2O_7$: Eu^{2+}, Dy^{3+} phosphors and the effect of sintering temperature. *Ceram. Int.* **48**, 5397–5403. https://doi.org/10.1016/j.ceramint.2021.11.083 (2022).
7. Homayoni, H. et al. X-ray excited luminescence and persistent luminescence of $Sr_2MgSi_2O_7$: Eu^{2+}, Dy^{3+} and their associations with synthesis conditions. *J. Lumin.* **198**, 132–137. https://doi.org/10.1016/j.jlumin.2018.02.042 (2018).
8. Pan, L. et al. Optimization method for blue $Sr_2MgSi_2O_7$: Eu^{2+}, Dy^{3+} phosphors produced by microwave synthesis route. *J. Alloys Compd.* **737**, 39–45. https://doi.org/10.1016/j.jallcom.2017.11.343 (2018).
9. Zhang, C., Gong, X. Y. & Deng, C. Y. The phase transition of color-tunable long afterglow phosphors $Sr_{1.94-x}Ba_xMgSi_2O_7$: $Eu^{2+}_{0.01}$, $Dy^{3+}_{0.05}$. *J. Alloys Compd.* **657**, 436–442. https://doi.org/10.1016/j.jallcom.2015.10.093 (2016).
10. Zhou, Z. et al. New viewpoint about the effects of boric acid on luminous intensity of $Sr_2MgSi_2O_7$: Eu, dy. *Mater. Res. Express* **6**, 086205. https://doi.org/10.1088/2053-1591/ab1dd0 (2019).
11. Wu, H., Hu, Y., Wang, Y., Kang, F. & Mou, Z. Investigation on Eu^{3+} doped $Sr_2MgSi_2O_7$ red-emitting phosphors for white-light-emitting diodes. *Opt. Laser Technol.* **43**, 1104–1110. https://doi.org/10.1016/j.optlastec.2011.02.006 (2011).
12. Li, Y., Wang, Y., Xu, X. & Gong, Y. Effects of non-stoichiometry on crystallinity, photoluminescence and afterglow properties of $Sr_2MgSi_2O_7$: Eu^{2+}, Dy^{3+} phosphors. *J. Lumin.* **129**, 1230–1234. https://doi.org/10.1016/j.jlumin.2009.06.014 (2009).
13. Jiao, H. Y., LiMao, C. R., Chen, Q., Wang, P. Y. & Cai, R. C. Enhancement of red emission intensity of $Ca_2Al_2SiO_7$: Eu^{3+} phosphor by MoO_3 doping or excess SiO_2 addition for application to white leds. *Mater. Sci. Eng.* **292**, 012058. https://doi.org/10.1088/1757-899X/292/1/012058 (2018). IOP Conf. Ser.

14. Zhang, C., Gong, X. Y., Cui, R. R. & Deng, C. Y. Improvable luminescent properties by adjusting silicium-calcium stoichiometric ratio in long afterglow phosphors $Ca_{1.94}MgSi_2O_7$: $Eu^{2+}{}_{0.01}$, $Dy^{3+}{}_{0.05}$. *J. Alloys Compd.* **658**, 898–903. https://doi.org/10.1016/j.jallcom.2015.10.209 (2016).
15. Yang, L. et al. Recent progress in inorganic afterglow materials: Mechanisms, persistent luminescent properties, modulating methods, and bioimaging applications. *Adv. Opt. Mater.*. https://doi.org/10.1002/adom.202202382 (2023).
16. Zeng, P., Wei, X., Yin, M. & Chen, Y. Investigation of the long afterglow mechanism in $SrAl_2O_4$: Eu^{2+}/Dy^{3+} by optically stimulated luminescence and thermoluminescence. *J. Lumin.* **199**, 400–406. https://doi.org/10.1016/j.jlumin.2018.03.088 (2018).
17. Yang, X., Waterhouse, G. I. N. & Lu, S. Yu. Recent advances in the design of afterglow materials: Mechanisms, structural regulation strategies and applications. *Chem. Soc. Rev.* **52**, 8005–8058. https://doi.org/10.1039/D2CS00993E (2023).
18. Kresse, G. & Hafner, J. Ab initio molecular dynamics for liquid metals. *Phys. Rev. B.* **47**, 558. https://doi.org/10.1103/PhysRevB.47.558 (1993).
19. Kresse, G. & Furthmüller, J. Efficient iterative schemes for Ab initio total-energy calculations using a plane-wave basis set. *Phys. Rev. B* **54**, 11169. https://doi.org/10.1103/PhysRevB.54.11169 (1996).
20. Perdew, J. P., Burke, K. & Ernzerhof, M. Generalized gradient approximation made simple. *Phys. Rev. Lett.* **77** 3865–3868. https://doi.org/10.1103/PhysRevLett.77.3865 (1996).
21. Tran, F. & Blaha, P. Accurate band gaps of semiconductors and insulators with a semilocal exchange-correlation potential. *Phys. Rev. Lett.* **102**, 226401. https://doi.org/10.1103/PhysRevLett.102.226401 (2009).
22. Pan, W. & Ning, G. Synthesis and luminescence properties of $Sr_3MgSi_2O_8$: Eu^{2+}, Dy^{3+} by a novel silica-nanocoating method. *Sens. Actuat A Phys.* **139**, 318–322. https://doi.org/10.1016/j.sna.2006.12.021 (2007).
23. Yu, H. et al. Green light emission by Ce^{3+} and Tb^{3+} co-doped $Sr_3MgSi_2O_8$ phosphors for potential application in ultraviolet whitelight-emitting diodes. *Opt. Laser Technol.* **44**, 2306–2311. https://doi.org/10.1016/j.optlastec.2012.02.005 (2012).
24. Chen, Y., Zhou, B., Sun, Q., Wang, Y. & Yan, B. Synthesis and luminescence properties of $Sr_3MgSi_2O_8$: Ce^{3+}, Tb^{3+} for application in near ultraviolet excitable white light-emitting-diodes. *Superlattice Microstruct.* **100**, 158–167. https://doi.org/10.1016/j.spmi.2016.09.017 (2016).
25. Brindley, G. W. & Hayami, R. Kinetics and mechanism of formation of forsterite (Mg_2SiO_4) by solid state reaction of MgO and SiO_2. *Philos. Mag.* **12**, 505–514. https://doi.org/10.1080/14786436508218896 (1965).
26. Gong, Y. et al. The persistent energy transfer of Eu^{2+} and Mn^{2+} and the thermoluminescence properties of long-lasting phosphor $Sr_3MgSi_2O_8$: Eu^{2+}, Mn^{2+}, Dy^{3+}. *Opt. Mater.* **33**, 1781–1785. https://doi.org/10.1016/j.optmat.2011.06.015 (2011).
27. Hai, O. et al. Effect of cooling rate on the microstructure and luminescence properties of $Sr_2MgSi_2O_7$: Eu^{2+}, Dy^{3+} materials. *Luminescence* **32**, 1442–1447. https://doi.org/10.1002/bio.3343 (2017).
28. Reddy, L. A review of the efficiency of white light (or Other) emissions in singly and Co-Doped Dy^{3+} ions in different host (Phosphate, silicate, aluminate. *Mater. J. Fluoresc.* **33**, 2181–2192. https://doi.org/10.1007/s10895-023-03250-y (2023).
29. Li, M. et al. Tunable luminescence in $Sr_2MgSi_2O_7$: Tb^{3+}, Eu^{3+} phosphors based on energy transfer. *Materials* **10**, 227. https://doi.org/10.3390/ma10030227 (2017).
30. Kunimoto, T., Honma, T., Ohmi, K., Okubo, S. & Ohta, H. Detailed impurity phase investigation by X-ray absorption fine structure and Electron spin resonance analyses in synthesis of $CaMgSi_2O_6$: Eu phosphor. *J. Appl. Phys.* **52**, 042402. https://doi.org/10.7567/JJAP.52.042402 (2013).
31. Li, Z. et al. Mechanism of long afterglow in $SrAl_2O_4$: Eu phosphors. *Ceram. Int.*. https://doi.org/10.1016/j.ceramint.2021.08.193 (2021).
32. Hai, O. et al. Insights into the element gradient in the grain and luminescence mechanism of the long afterglow material $Sr_2MgSi_2O_7$: Eu^{2+}, Dy^{3+}. *J. Alloys Compd.* **779**, 892–899. https://doi.org/10.1016/j.jallcom.2018.11.163 (2019).
33. Qu, B. Y., Zhang, B., Wang, L., Zhou, R. L. & Zeng, X. C. Mechanistic study of the persistent luminescence of $CaAl_2O_4$: Eu, Nd. *Chem. Mater.* **27**, 2195–2202. https://doi.org/10.1021/acs.chemmater.5b00288 (2015).
34. Yang, X., Tang, B. & Cao, X. The roles of Dopant concentration and defect States in the optical properties of $Sr_2MgSi_2O_7$: Eu^{2+}, Dy^{3+}. *J. Alloys Compd.* **949**, 169841. https://doi.org/10.1016/j.jallcom.2023.169841 (2023).
35. Sahu, I. P., Bisen, D. P., Brahme, N. & Ganjir, M. Enhancement of the photoluminescence and long afterglow properties of $Sr_2MgSi_2O_7$: Eu^{2+} phosphor by Dy^{3+} co-doping. *Luminescence* **30**, 1318–1325. https://doi.org/10.1002/bio.2900 (2015).
36. Chang, C. et al. Photoluminescence and afterglow behavior of Eu^{2+}, Dy^{3+} and Eu^{3+}, Dy^{3+} in $Sr_3Al_2O_6$ matrix. *J. Lumin.* **130**, 347–350. https://doi.org/10.1016/j.jlumin.2009.09.016 (2010).
37. Aitasalo, T. et al. Synchrotron radiation investigations of the $Sr_2MgSi_2O_7$: Eu^{2+}, R^{3+} persistent luminescence materials. *J. Rare Earth* **27**, 529–538. https://doi.org/10.1016/S1002-0721(08)60283-5 (2009).

Author contributions

C.Z.: Conceptualization, Data curation, Formal analysis, Investigation, Writing – original draft, Writing – review & editing. L.W.: Data curation, Formal analysis, Investigation, Writing – review & editing. R.C.: Investigation, Writing – review & editing. Q.L.: Investigation, Writing – review & editing. C.D.: Software, Funding acquisition, Project administration, Writing – review & editing. J.L.: Conceptualization, Investigation, Methodology, Supervision, Writing – review & editing.

Declarations

Competing interests

The authors declare no competing interests.

Additional information

Correspondence and requests for materials should be addressed to C.Z., C.D. or J.L.

Reprints and permissions information is available at www.nature.com/reprints.

Publisher's note Springer Nature remains neutral with regard to jurisdictional claims in published maps and institutional affiliations.